Geophysical Journal International

Geophys. J. Int. (2013) **195,** 1721–1729
Advance Access publication 2013 September 9

doi: 10.1093/gji/ggt319

Reconciling discrepancies among estimates of small-scale mantle heterogeneity from *PKP* precursors

Nicholas J. Mancinelli and Peter M. Shearer

Scripps Institution of Oceanography, University of California, San Diego, 9500 *Gilman Drive, La Jolla, CA* 92093, *USA. E-mail: njmancin@ucsd.edu*

Accepted 2013 August 6. Received 2013 July 31; in original form 2013 May 22

SUMMARY

We stack amplitudes of over 10 000 high-frequency (∼1 Hz) *PKP* precursor waveforms, amassed from broad-band global seismic data with source–receiver distances between 120° and 145° recorded from 1990 to 2012. We forward model the stacked precursor envelope with an energy-conserving, multiple-scattering algorithm to find that an rms velocity perturbation of ∼0.1 per cent fits the data reasonably well, in agreement with Margerin & Nolet. Similar results can be obtained using single-scattering (Born) theory, given the relatively weak scattering produced by our preferred model. The ramp-like increase in *PKP* precursor amplitudes with time is best fit with whole mantle scattering rather than models where scattering is restricted to the core–mantle boundary. Correctly modelling the relative amplitude of *PKP* precursor amplitudes compared to *PKPdf* requires taking into account the pulse broadening and coda of *PKPdf*, which can be done either empirically or by including a strongly scattering lithospheric layer in the multiple-scattering code. Several mantle scattering models proposed to explain other scattered seismic phases predict *PKP* precursor amplitudes much larger than those observed.

Key words: Mantle processes; Composition of the mantle; Coda waves; Wave scattering and diffraction.

1 INTRODUCTION

Seismic scattering by small-scale heterogeneities in Earth's lowermost mantle causes short-period energy to arrive before the core phase *PKP* (Cleary & Haddon 1972). The strength and depth extent of such heterogeneity, however, still remains a subject of debate. Doornbos & Vlaar (1973) originally argued for volumetric scatterers distributed 900 km above the core–mantle boundary (CMB), but Haddon & Cleary (1974) preferred to restrict the heterogeneity to a 200-km-thick layer above the CMB. Later, Doornbos (1978) used perturbation theory to show that topography on the CMB could describe the precursor amplitudes and onset times. Discrepancies among these early studies are difficult to reconcile because of possible selection biases on the then limited number of available seismograms. [See Shearer (2007) for a more detailed history of this subject.]

Two more recent analyses of *PKP* precursors, Hedlin *et al.* (1997) and Margerin & Nolet (2003b), used global stacking techniques to elicit the time and range dependence of the precursor amplitudes. These two studies agreed that small-scale (∼10 km) heterogeneity distributed throughout the mantle explains the time dependence of observed *PKP* precursor amplitudes better than models where scattering is restricted to the D″ region. Margerin & Nolet (2003b), however, contested the 1 per cent rms velocity perturbation originally proposed by Hedlin *et al.* (1997) to explain the strength of the precursors, arguing instead for a much weaker value between 0.1 and 0.2 per cent.

The reason for the discrepancy between the two studies has remained unclear, including whether it reflects different data processing choices or differences in theoretical modelling of the scattering. Hedlin *et al.* (1997) employed a single-scattering theory (e.g. Chernov 1960) to sum Born scattering kernels for various mantle depth layers while Margerin & Nolet (2003b) used a multiple-scattering approach. However, for the 0.1 per cent velocity perturbation proposed by Margerin & Nolet (2003b), the scattering should be relatively weak, so there should not be a large difference between single and multiple scattering theories.

To resolve this disagreement, we perform a similar but independent analysis on a much larger data set of *PKP* precursors, modelling their stacked amplitudes using a Monte Carlo seismic phonon algorithm (e.g. Shearer & Earle 2004, 2008; Peng *et al.* 2008) which conserves energy and allows for multiple scattering. Our best-fitting model agrees with Margerin & Nolet (2003b), yet we also find that a single-scattering approximation achieves similar results. We confirm that *PKP* observations favour whole mantle scattering rather than scattering from just the CMB or the D″ layer and show how strong scattering in the lithosphere can roughly explain observed *PKPdf* waveform broadening. Observed *PKP* precursor amplitudes provide strong constraints on lower mantle scattering strength, and we show how two models proposed to explain other high-frequency scattered phases predict *PKP* precursor amplitudes much higher than those observed. Finally, we discuss the implications of these results for whole-Earth scattering profiles and geodynamic and geochemical models.

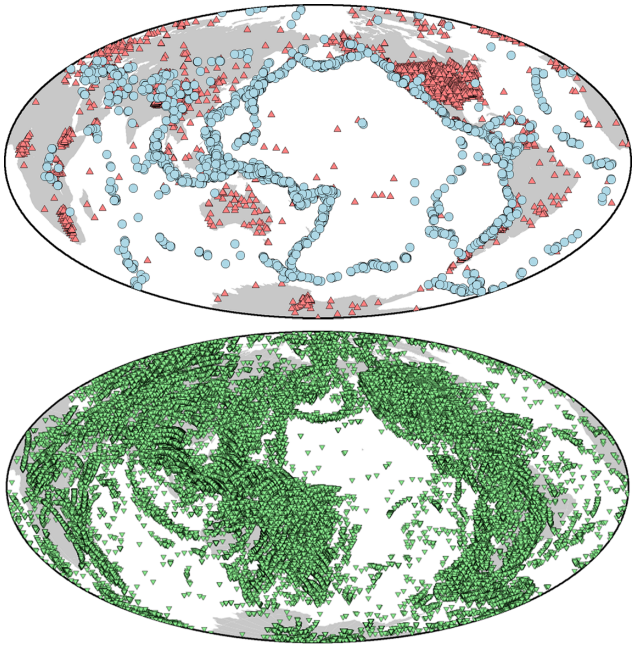

Figure 1. Top: Hammer projection showing source (blue circles) and receiver (red triangles) locations for waveforms analysed in this study. Bottom: The green markers show approximate CMB entry–exit points.

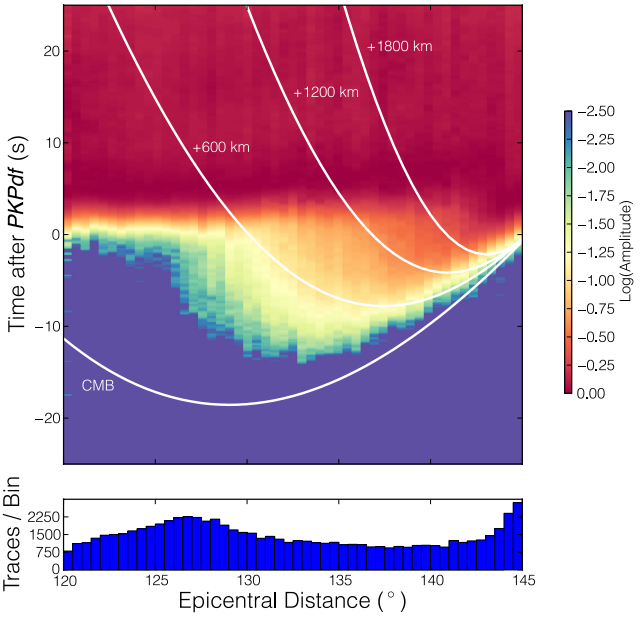

Figure 2. Top panel: Data stack showing the time and range dependence of *PKP* precursors. The time-series are sampled at 20 Hz and are stacked in 0.5° range bins. Times are relative to the *PKPdf* onset and amplitudes are relative to the *PKP*(*df,cd*) maximum at each range. The white curves show earliest possible ray-theoretical arrival times for energy scattered above the CMB (units in km above the CMB). Bottom panel: Number of recordings stacked in each range bin.

2 DATA SELECTION AND STACKING

Since Margerin & Nolet (2003b), the amount of global seismic data has increased enormously. Using the Standing Order for Data (Owens *et al.* 2004) to download data from the Incorporated Research Institutions for Seismology (IRIS), we obtained more than 150 000 broad-band *PKP* waveforms recorded at epicentral distances between 120° and 145° with $M_w \geq 5.7$ for shallow events (depth <50 km) and with $M_w \geq 5.5$ for deeper events. Fig. 1 shows the source–receiver distribution of the data used, as well as their associated CMB entry–exit points where the earliest arriving precursor energy is likely to be scattered.

Prior to stacking, we bandpass filter the traces from 0.7 to 2.5 Hz and align them on their *PKPdf* arrival times as calculated from the Preliminary Reference Earth Model (PREM; Dziewonski & Anderson 1981). After alignment, we reject traces that exhibit low signal-to-noise ratios. Next, we compute the envelope function for each trace and subtract the average pre-event noise power. Because the energy arriving 0–20 s before the main arrival is of primary interest, we define the pre-event window to be 20–60 s before *PKPdf*. Finally, we normalize each trace by the maximum amplitude arriving between 0 and 5 s (i.e. the *PKP* arrival) and sum them in 0.5° range bins. Roughly 1000 seismograms contribute to the final stack in each range bin. Fig. 2 shows the time and range dependence of the precursor amplitudes, with the white curves showing ray-theoretical scattering onset times as a function of scattering depth.

Although Fig. 2 is a pleasing image, it may not accurately represent globally averaged *PKP* precursor behaviour. As Fig. 1 makes clear, the source and receiver distribution is very non-uniform and previous studies have suggested that there exist considerable 3-D variations in heterogeneity strength. Vidale & Hedlin (1998), for instance, found exceptionally strong scattering near the CMB beneath the Pacific Ocean north of Tonga. Hedlin & Shearer (2000) identified strongly scattering areas beneath central Africa, parts of North America and north of India. Margerin & Nolet (2003b) constructed substacks based on region and observed stronger-than-average stacked envelopes for the Tonga-Eurasia corridor. Using short-period *PcP* reflections, Rost & Thomas (2010) found a *P*-wave reflector at 110 km above the CMB beneath the Kenai Peninsula.

To reduce the possible biasing effects of the non-uniform station coverage, including the high concentration of stations in the United States and Europe, we apply a weighting scheme that emphasizes data from poorly sampled regions of the lower mantle. For an individual trace recorded at location (θ, ϕ), we count the total number of traces, N, within a certain angular distance, Δ, from (θ, ϕ). During the stacking procedure, we then weight each trace by $1/N$, so that receiver-sparse areas influence the final stack as much as receiver-dense areas. As shown in Fig. 3, we experiment with different Δ values to find that the main features of the precursor envelope remain largely unaffected by the weighting. This strengthens the notion that *PKP* precursors are a global feature, despite some degree of lateral variability. For higher choices of Δ, the stacked precursor envelope becomes less smooth. We attribute this behaviour to the strong downweighting of most traces in the stack, excepting those few with rare source–receiver paths. Upon stacking, these rare traces are insufficient in number to form a smooth envelope.

In addition to reducing bias due to non-uniform data coverage, we would like to estimate error bars for the *PKP* precursor amplitudes, which ideally should include the effects of our limited data coverage rather than just variability in the raw data set. Thus, instead of treating each trace as an independent measurement, we construct multiple substacks that group similar ray geometries and treat these as statistically independent measurements. More specifically, we divide Earth's surface into 12 equal-area cells and group traces that have traversed along similar corridors through the Earth. Because we group traces based on both source and receiver location, there are 144 possible combinations. However, only about 30 of these groups are populated because source–receiver distances for *PKP*

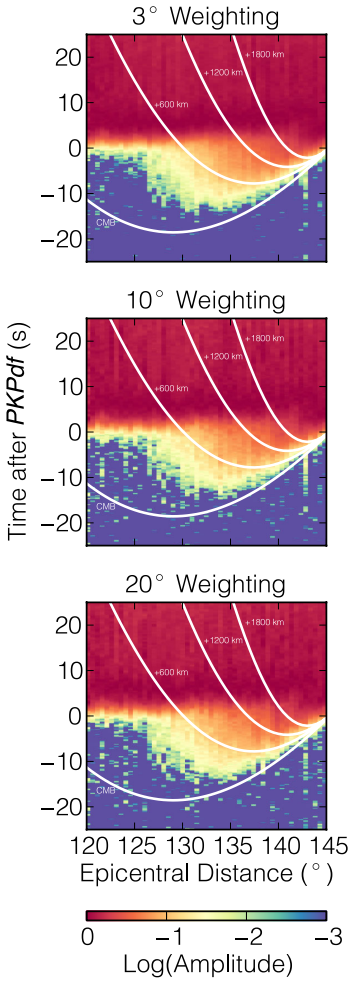

Figure 3. Comparison of different weighting schemes used to elicit globally averaged precursor amplitudes.

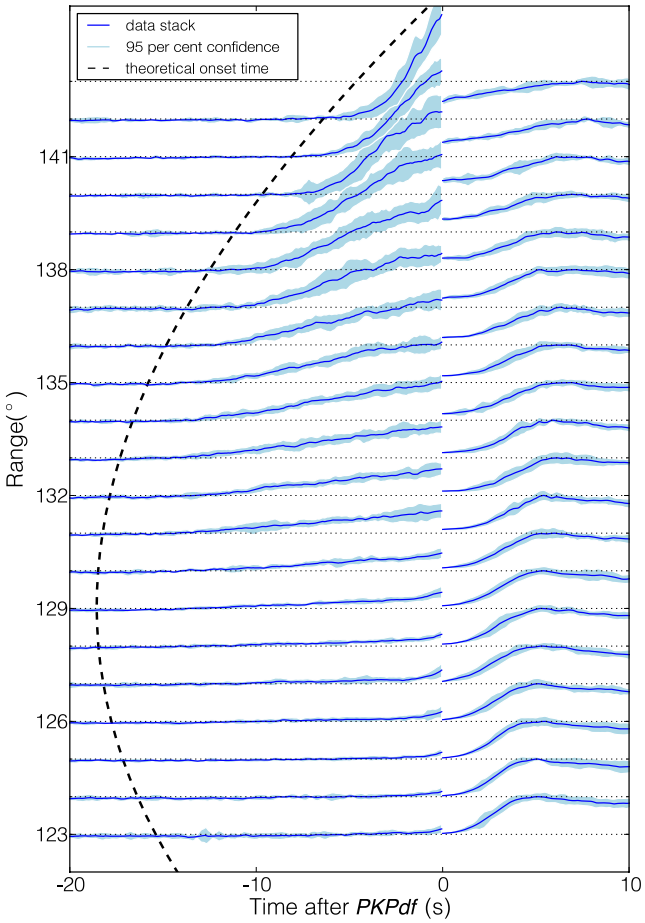

Figure 4. Vertical cross-sections of the data stack with 95 per cent confidence limits from bootstrap resampling. To enhance visibility of the precursors, the stacks are scaled up by a factor of five at negative times. The dashed line shows the ray-theoretical onset time for waves scattered at the CMB.

precursors are limited to between 120° and 145°. To compute error bars, we apply a bootstrap resampling algorithm that repeatedly averages random combinations of these 30 populated groups. The resulting 95 per cent confidence intervals are shown in Fig. 4.

Although our data set is much larger than those used in previous studies, our stacked *PKP* precursor amplitudes are quite similar. With increasing time, the observed envelope emerges rather slowly after the ray-theoretical onset (plotted in Fig. 4). Since the main phase ramps-up in a similarly gradual way, this behaviour may result from waveform broadening effects caused by strong heterogeneity in the lithosphere. With increasing range, a robust precursor signal emerges from the noise at about 125° and increases gradually until 143°, where geometrical focusing near the b-caustic makes interpretation difficult.

We explored alternatives to the alignment strategy described above. Since PREM is a 1-D earth model, we do not expect all of the traces to line up perfectly with the PREM predicted traveltime curve. Large-scale lateral heterogeneity results in a traveltime spread of about ±1s, thereby limiting the time resolution of the data stack. Attempts to align the traces with an autopicking algorithm or a maximum amplitude criterion were abandoned since they did not produce appreciatively clearer results and in some cases produced artefacts.

Our stacks agree with previous studies, so it is very unlikely that the factor-of-10 discrepancy between Hedlin *et al.* (1997) and Margerin & Nolet (2003b) arises from data selection biases or from subtleties in their stacking procedures. In the next section, we explore the possibility that the disagreement arises from differences in modelling assumptions.

3 SEISMIC PHONON MODELS

We use the Monte Carlo seismic phonon method described by Shearer & Earle (2004) to forward model the *PKP* precursor amplitudes. Though the details of numerical implementation differ, this algorithm is similar to the one developed in Margerin & Nolet (2003a). In brief, the method tracks individual energy particles sprayed from a seismic source located at the surface as they travel along trajectories from a large table of pre-computed ray paths. Upon entering a scattering volume, a random path length is assigned to the particle. Once the particle exceeds that path length, a scattering event occurs and a random new direction and path length are assigned. When the particle returns to the surface, it is summed in an appropriate time-range bin. The method is designed such that, when the number of summed particles becomes large, the distribution of path lengths is exponential with mean value l (since the probability of scattering along the ray path is constant) and the distribution of scattering angles matches the basic scattering patterns given by Sato & Fehler (1997).

This method obeys energy conservation, allows for multiple scattering, and naturally accounts for geometrical spreading and out-of-plane scattering effects. For computational efficiency, we initially consider *P*-to-*P* scattering only and restrict the seismic source to spray particles only along ray parameters, p, between 0 and 0.116 s km^{-1}. In the following section, we will discuss how additional scattering (*P*-to-*S* and *S*-to-*P*) in the lithosphere may help describe the slow decay of *PKP* coda.

We divide the mantle into three concentric scattering volumes, each described by a mean-free path, l. The heterogeneity power spectrum in each volume is modelled with an exponential autocorrelation function (see Sato & Fehler 1997), parametrized by rms velocity perturbation, ϵ, and correlation length, a. The models assume a velocity–density scaling factor, ν, of 0.8 to be consistent with previous studies. This parameter controls the amount of backscattering and should not significantly affect our results since *PKP* precursors are generated by near-forward scattering. To be certain that this is the case, we rerun our calculations with $\nu = 0$, that is, with no density perturbations, and find that the synthetics are unaffected. Presumably the choice of ν would be more relevant in the modelling of phases such as *PKKP* where backscattering is dominant. We determine the wavenumber from 1.3 Hz, the dominant frequency of the data, and the mean background velocity of each volume. The pre-computed ray paths are based on a modified version of IASP91 (Kennett & Engdahl 1991) where the sharp corner in the velocity profile at 2740 km depth is slightly smoothed.

The relatively weak scattering we assume for the lower mantle does not produce much pulse broadening or coda in *PKPdf*, that is, the *PKPdf* pulses are much sharper than those seen in the data stacks. It is likely that the main source of *PKPdf* pulse broadening and coda is strong scattering in the lithosphere. Because *PKP* precursor ray paths also traverse the lithosphere, they should be similarly affected. Thus, correctly modelling the relative amplitudes of *PKP* precursors compared to *PKPdf* requires taking these pulse broadening effects into account, which in general will tend to increase precursor amplitudes compared to the peak *PKPdf* amplitude. This is most easily done by convolving the seismic phonon results, in power, with a empirical function that roughly matches the *PKPdf* observations. Later we will show how similar results can be obtained by explicitly including strong scattering in the lithosphere.

It is currently impractical to perform a rigorous grid search for a and ϵ because of the length of time required for each forward model. Through trial and error, we find that heterogeneity distributed throughout the entire mantle with $\epsilon = 0.1$ per cent and $a = 6$ km closely agrees with the data stack, as shown in Fig. 5. Smaller values of a (e.g. 2 km) tend to overpredict amplitudes at short ranges and underpredict amplitudes at long ranges; larger values of a (e.g. 18 km) exhibit the opposite behaviour. Fig. 6 illustrates this effect of a on the synthetics.

This model assumes an inner core Q_α of 360 (Bhattacharyya *et al.* 1993). More recently, Monnereau *et al.* (2010) observed that the inner core exhibits hemispherical variations in both v_p and Q_α. The centre of the low attenuation ($Q_\alpha = 410$) hemisphere is beneath the Americas and the high attenuation hemisphere ($Q_\alpha = 160$), beneath the Indian Ocean. We test how these other Q-values would affect our preferred model; we would have to adjust ϵ by less than ± 15 per cent to achieve equally good fits. The CD branch, which is unaffected by inner core attenuation, arrives just after the DF branch. In the case of strong core attenuation, the CD arrival takes the place of DF as the reference phase.

Fig. 7 shows the preferred models from Hedlin *et al.* (1997) and Margerin & Nolet (2003b) as calculated by the seismic phonon method. The model proposed by Hedlin *et al.* (1997) overpredicts the observed amplitudes by a margin much larger than allowed by the data uncertainties whereas the model put forth by Margerin & Nolet (2003b) provides a reasonable fit. To test whether the poor fit of Hedlin *et al.* (1997) comes from using a single-scattering approach, we restrict the seismic phonon algorithm to output only singly scattered particles. We find, however, that 90 per cent of the energy arriving near *PKP* experiences zero scattering events (these comprise the direct wave); 9 per cent are scattered once (the Born term) and the remaining 1 per cent are scattered multiple times. Therefore, a single-scattering assumption is unlikely to cause a factor of 10 underprediction of the scattered amplitudes.

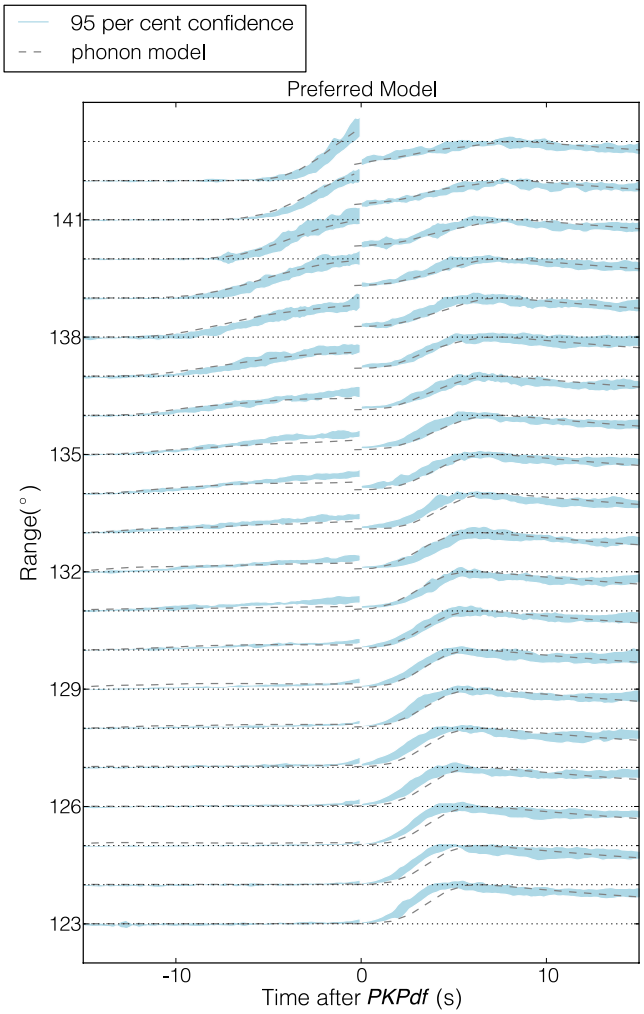

Figure 5. Preferred model plotted against the 95 per cent confidence intervals of the data stack. Precursors are enhanced by a factor of three.

Why, then, do our results disagree with those published by Hedlin *et al.* (1997)? We obtained a copy of the Born scattering code used by Hedlin *et al.* (1997) and were able to identify two problems that together resulted in a systematic underprediction of the Born kernels by about a factor of eight. Specifically, the time bins in the numerical integration scheme were incorrectly normalized and the geometrical spreading factor was miscalculated for the second leg of each scattered wave. This accounts for the discrepancy. The overall shapes of the kernels, however, are not significantly altered by this bug, so the Hedlin *et al.* (1997) conclusion that whole-mantle scattering fits the data better than CMB-only scattering remains valid. We confirm this result in our phonon calculations by restricting

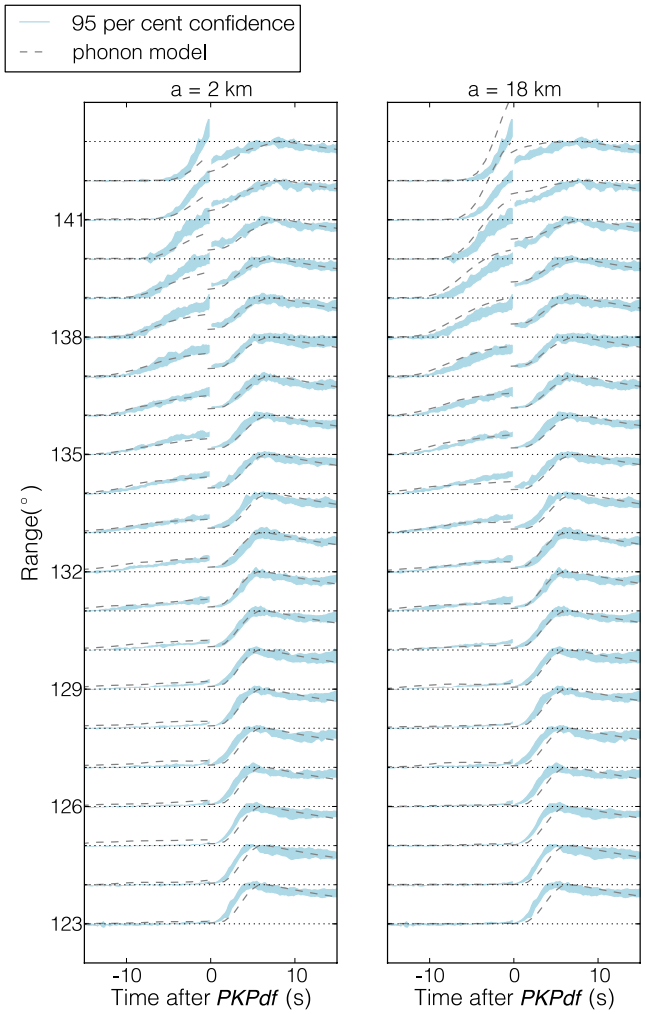

Figure 6. A demonstration of how these data are able to constrain correlation length. Left-hand column: An exponential model with $a = 2$ km and $\epsilon = 0.2$ per cent underpredicts the precursor amplitude at high ranges. Right-hand coulmn: An exponential model with $a = 18$ km and $\epsilon = 0.2$ per cent overpredicts the precursor amplitudes at high ranges.

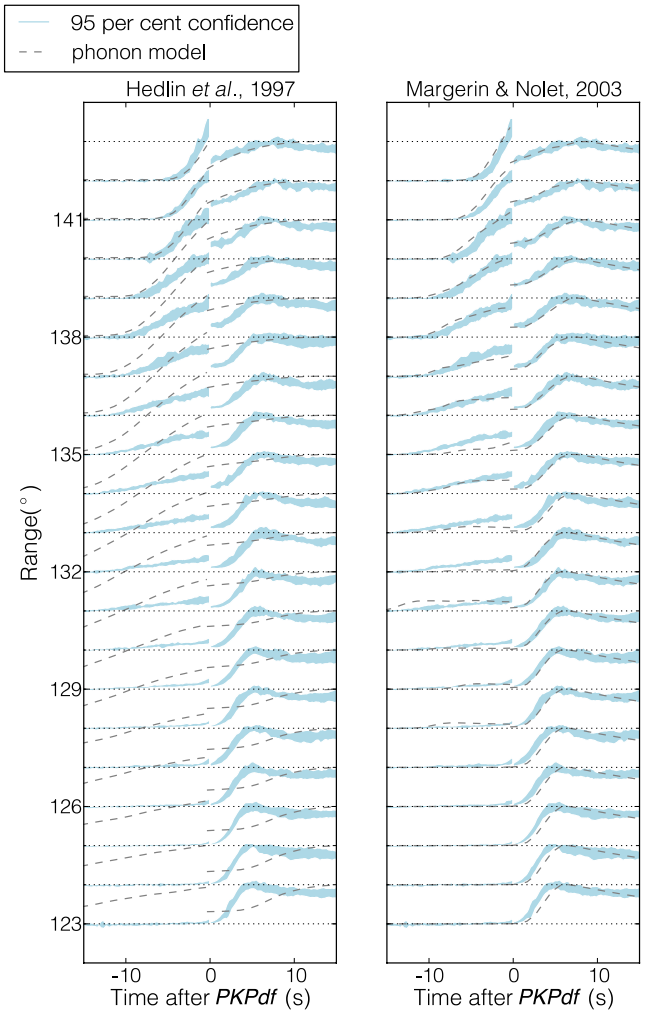

Figure 7. Synthetics generated by the seismic phonon algorithm plotted against our data stacks. The left-side column shows the Hedlin *et al.* (1997) preferred values of a and ϵ, whereas the right-side column shows the Margerin & Nolet (2003b) values. To enhance visibility of the precursors, the curves are magnified by a factor of three at negative times.

scattering to a 200-km-thick region above the CMB and choosing ϵ and a until we achieve a reasonable fit. Though the differences are admittedly subtle, the best-fitting CMB-only model shown in Fig. 8 rises more steeply than the data, then flattens while the data continue to rise, and underpredicts the observed amplitudes near the *PKPdf* onset by a margin larger than the uncertainty estimates allow. If we increase ϵ to fit the later arriving precursors, the model increasingly overpredicts the earliest arriving amplitudes. This was previously noted by both Hedlin *et al.* (1997) and Margerin & Nolet (2003b).

Before moving on, we should emphasize that this result is based upon data that are narrow-band-filtered around 10 km. Features at longer or shorter scale lengths may—and probably do—exist, but these filtered data are not sensitive to them. As noted by Cormier (2000), the distinctness of D″ may disappear when one only considers the high-frequency part of the spectrum. We have chosen to work in this frequency band for the sake of resolving the disagreement between Hedlin *et al.* (1997) and Margerin & Nolet (2003b), but future work should make an effort to probe longer and shorter wavelengths.

We should also note that this method is subject to the limitations of ray theory, and—in its current form—is unable to model diffracted waves. We hope that we have avoided potential problems with this approximation by working in a sufficiently high-frequency band, which is supported by the non-observation of the *PKP* diffracted wave near the b-caustic in our data stacks. Another potential issue is the amplification of the waves scattered in and out of the b-caustic, which this method treats via ray (or rather, particle) densities. We justify this approach because the algorithm is limited to a finite number of particles, and thus it is impossible to get infinite energy near a caustic. As computational capabilities improve, it would be useful to see how well global 3-D numerical simulations of the wave equation agree with this high-frequency approximation.

4 INCLUDING LITHOSPHERIC SCATTERING

As shown by the white traveltimes curves in Fig. 2, scattered energy near the b-caustic may arrive after the *PKPdf* onset. If these amplitudes could be accurately observed, one could make stronger conclusions about the depth extent of small-scale structure in the

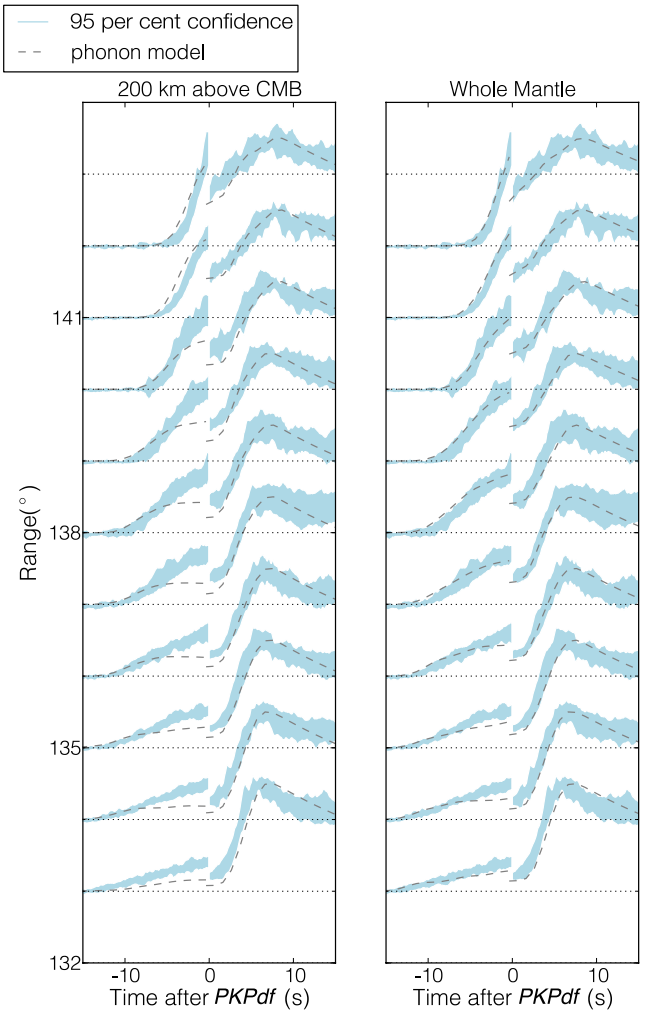

Figure 8. A comparison of a best-fitting whole-mantle scattering model with a best-fitting CMB scattering model. To highlight the difference between the two fits, the curves are magnified by a factor of three at negative times and by a factor of 1.5 at positive times.

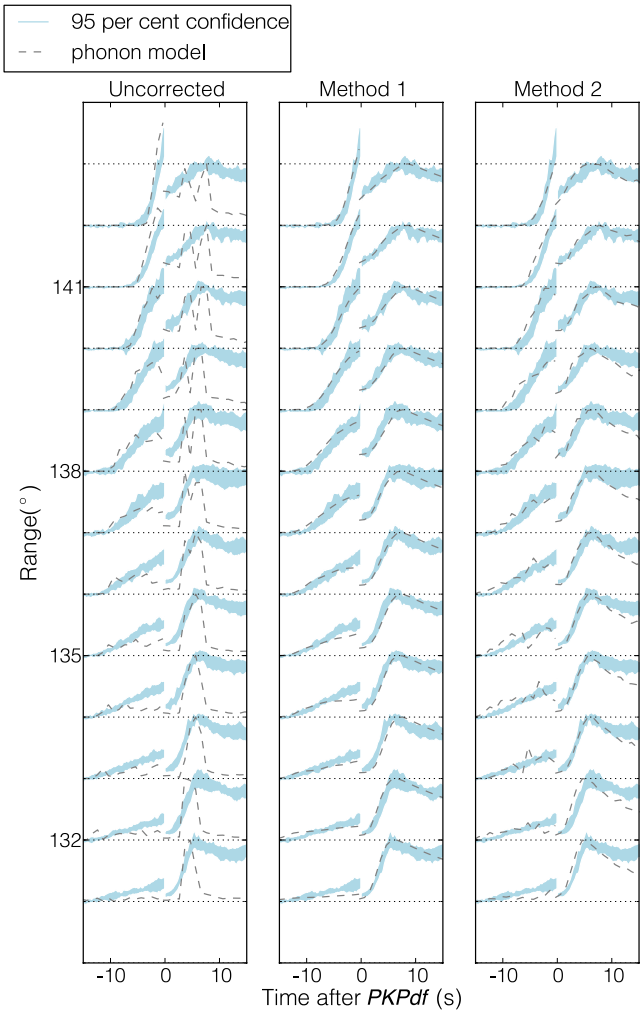

Figure 9. Two methods that account for strong scattering in the lithosphere. The leftmost column shows the uncorrected output of our preferred seismic phonon model. The central column shows the broadened amplitudes after convolution with an empirical function. The rightmost column shows broadened amplitudes obtained by direct modelling with the seismic phonon method. The precursors are enhanced by a factor of three.

mid-mantle. However, Hedlin & Shearer (2002) showed that in practice the large statistical variability in *PKP* coda makes constraining mid-mantle heterogeneity difficult. It is believed that much of this variability is caused by incoherence in depth phase arrivals between stacked events. In addition, the observed waveforms pass through the strongly heterogeneous lithosphere, and the *PKPdf* branch traverses the inner core, which has been shown to scatter high frequencies (Cormier & Li 2002; Peng *et al.* 2008).

Although this study focuses primarily on fitting *PKP* precursors, we want our models to match, at least crudely, the coda shapes. Strong scattering in the lithosphere will spread energy out from both the *PKP* precursors and the main arrival. However, because the *PKP* precursors are already spread out in time, the result will be to increase the amplitude of the precursors relative to the peak *PKPdf* amplitude. This effect can double the relative precursor amplitude just before the onset of *PKPdf*, most notably at ranges where the precursor onset time is earliest.

To incorporate the effect of the lithosphere, we develop and compare two different approaches. Fig. 9 shows how each method affects the uncorrected amplitudes. The first approach, used previously to produce Figs 5, 7 and 8, simply entails a convolution, in power, of the seismic phonon output with an empirical function. In the second approach, the seismic phonon method explicitly models the lithospheric scattering. To the original three mantle volumes discussed in the previous section, we add a lithospheric scattering volume with $\epsilon = 4$ per cent and $a = 4$ km from 0–200 km depth. We also augment the scattering strength in the uppermost mantle volume (depth range 200–600 km) by increasing ϵ to 3 per cent. Improving upon the first approach, this method sprays particles for the full range of p and keeps track of P-to-S and S-to-P scattering. We like this approach because of its physical basis, but it is computationally expensive to sum over the full range of p for both P and S waves, often requiring hundreds of CPU hours to obtain an acceptably smooth result.

For this study, we have mainly used the convolution method because of its speed and simplicity. Ultimately, however, we would like to use the seismic phonon method to model the effects of whole Earth scattering on the full length of the *PKP* envelope. Cormier & Li (2002) suggested that scattering is the predominant attenuation mechanism of the inner core for the 0.02–2 Hz frequency band. If we relax the $Q_\alpha = 360$ assumption and instead use the Cormier & Li (2002) scattering model ($\epsilon = 8.4$ per cent, $a = 9.8$ km) in the uppermost 300 km of the inner core, the modelled precursor

amplitudes are not significantly affected. The change of inner core attenuation mechanism does, however, cause an amplitude increase in *PKP* coda, but this inner core scattering model produces less than 50 per cent of the coda amplitude observed in the data stack. The remaining coda power is most likely generated by scattering in the lithosphere.

5 DISCUSSION

5.1 Relevance to observations of *P* coda and *P* diff coda

PKP precursors are uniquely valuable to the study of deep small-scale structure because of their sensitivity to the lowermost mantle and because they arrive before the main phase rather than in its coda. However, as reviewed by Shearer (2007), there are a number of other scattered seismic phases that have at least some sensitivity to deep-Earth scattering.

Earle & Shearer (2001) modelled global stacks of *P* diff coda with a mantle containing evenly distributed fine-scale heterogeneity of $a = 2$ km and $\epsilon = 1$ per cent. Later, Shearer & Earle (2004) modelled *P*coda amplitudes between 30° and 90° using the seismic phonon method with $a = 8$ km and $\epsilon = 0.5$ per cent throughout the lower mantle. Though these two models are non-unique, they show that observations of *P* coda and *P* diff coda are compatible with whole-mantle scattering. However, these models have lower mantle velocity perturbations much stronger than the 0.1 per cent perturbations that we have shown are consistent with *PKP* precursor amplitudes. Thus, as shown in Fig. 10, both proposed models systematically overpredict the data amplitudes. The reason for this discrepancy is not clear and will require further study. The Earle & Shearer (2001) *P* diff coda study used a single-scattering theory and it is possible that strong scattering near the CMB could channel *P* diff scattered energy. *P* coda is dominated by strong scattering in the shallow Earth and it is possible that alternate models exist that could explain the data using only 0.1 per cent velocity perturbations in the lowermost mantle. Alternatively, scattering in the lower mantle may be anisotropic, with stronger scattering occurring for the more horizontally travelling rays contributing to *P* coda than for the more vertically travelling rays contributing to *PKP* precursors. An analysis of broad-band *PKP* waveforms by Cormier (1999) suggests that such anisotropy is unlikely to be present throughout the entire lower mantle, yet it may be a feature of the D″ layer. Our long-term objective is to find a self-consistent earth model that can adequately explain the amplitudes of all the main scattered phases.

5.2 Geodynamical interpretation

Though a and ϵ have clear relevance to the Earth's velocity structure, these parameters should also provide constraints on geodynamical models of the mantle. The small values for a required to produce short-period precursors imply that the heterogeneity is of chemical, rather than thermal, origin. Here, we identify possible avenues of interpretation.

(1) Slab recycling. Over geological timescales, the near-surface rock cycle continuously creates compositional heterogeneity in the form of oceanic crust and underlying depleted lithosphere; subduction transports this heterogeneity into the mantle (e.g. Stixrude & Lithgow-Bertelloni 2012). It has been proposed (e.g. Brandenburg & van Keken 2007) that subducted oceanic crust may accumulate at the base of the mantle to form the seismically observed large low shear velocity provinces (LLSVPs). However, mantle convection

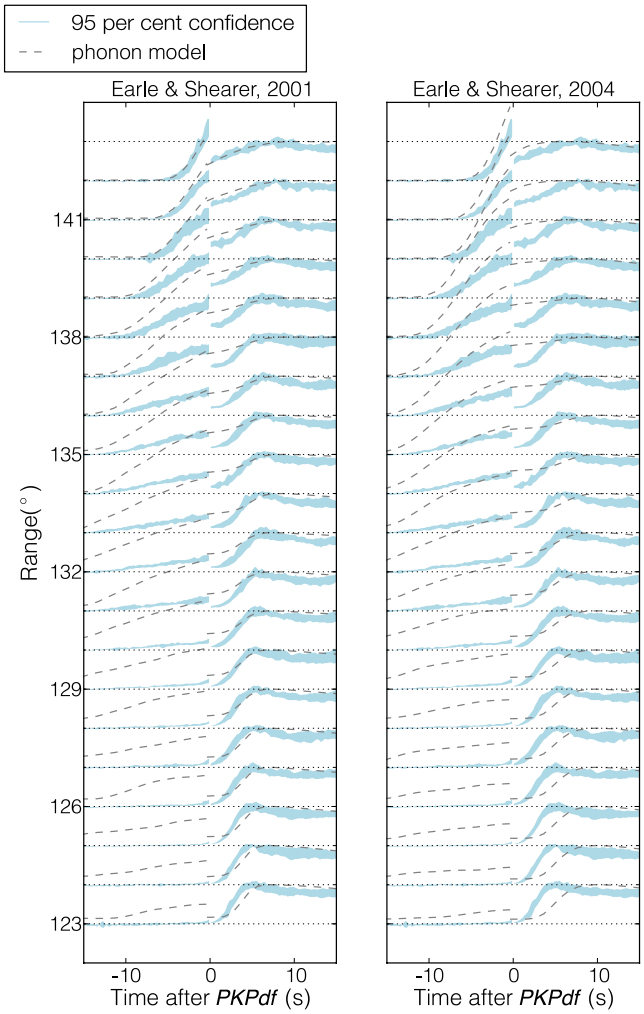

Figure 10. Seismic phonon predictions of preferred mantle scattering models from studies of *P* diff coda (left-hand column) and *P* coda (right-hand column). Convolution applied to correct for *PKPdf* broadening. The precursors are enhanced by a factor of three.

models by Li & McNamara (2013) suggest that subducted oceanic crust is viscously stirred into the mantle at quicker rates than such structures would be able to form, implying that this heterogeneity may be distributed more evenly throughout the mantle. Likewise, Kaneshima & Helffrich (2010) interpreted *S*-to-*P* scattering objects at mid-lower mantle depths (800–2200 km) as subducted and folded oceanic crust. Their observations support the notion that small-scale heterogeneity persists for billions of years despite convective stirring and is ubiquitous in the lower mantle.

(2) Primordial mantle material. A portion of this chemical heterogeneity could be interpreted as primordial material which, through mantle convection, has been sheared, refolded and interbedded with younger recycled material (e.g. Albarède 2005). Mixing models by Manga (1996) support this notion that geochemical reservoirs can persist in the mantle for gigayears, provided that they are 10–100 times more viscous than the surrounding mantle.

(3) LLSVP-related silicate melt or iron enriched mantle. Using short-period arrays, Frost *et al.* (2013) deterministically located small-scale scatters that produced *PKP* precursors on seismograms recorded by the Yellowknife Array. These scatterers cluster into a ridge above the CMB beneath South Africa, possibly composed of

dense residual material expelled to the edges of the LLSVP during convection.

(4) Small-scale variations in CMB topography. Although our preferred model contains heterogeneity uniformly distributed throughout the mantle, we cannot rule out contributions from CMB topography. Recently discovered rolling-hill structures on the CMB may have been formed by interactions between the outer core and the lowermost mantle (Sun *et al.* 2013). Admittedly, these features are more than an order of magnitude larger than the ∼10 km heterogeneities that would cause 1 Hz precursors, but such evidence for iron-rich structures at the base of the mantle raises the possibility that similar structures may exist at a smaller scale.

Absent from any of these interpretations is our preferred ϵ value of 0.1 per cent. This global average may represent the product of the volume fraction of heterogeneous material and the velocity perturbation (in per cent) of that material. To determine which, if any, of the above interpretations provides the most plausible explanation for small-scale compositional heterogeneity in the mantle requires an interdisciplinary approach that considers both mineral physics and convective mixing calculations.

6 CONCLUSION

In summary, we have constructed global stacks of *PKP* precursor amplitudes from all available broad-band seismograms recorded from 1990 to 2012 to find that they do not differ considerably from previous studies. We have modelled their envelopes using an energy-conserving, multiple-scattering approach to show, in accordance with Margerin & Nolet (2003b), that an rms perturbation of ∼0.1 per cent explains the data. We have reconciled this result with the 1 per cent value published by Hedlin *et al.* (1997) by finding a scaling error in their code. We have developed two separate methods to account for strong lithospheric scattering and have confirmed that small-scale (∼10 km) heterogeneity is not confined to a 200-km-layer above the CMB. These results provide constraints on geodynamic and geochemical models of the lower mantle.

ACKNOWLEDGEMENTS

This research was supported by National Science Foundation grant EAR1111111. The authors thank Vernon Cormier, an anonymous reviewer and the editor for suggestions that improved the quality of this manuscript. We wish to acknowledge the facilities of the IRIS Data Management System, and specifically the IRIS Data Management Center, which were used for access to waveform and metadata required in this study. The IRIS DMS is funded through the National Science Foundation under Cooperative Agreement EAR-1063471.

REFERENCES

Albarède, F., 2005. *The Survival of Mantle Geochemical Heterogeneities,* pp. 27–46, American Geophysical Union.

Bhattacharyya, J., Shearer, P. & Masters, G., 1993. Inner core attenuation from short-period PKP(BC) versus PKP(DF) waveforms, *Geophys. J. Int.,* **114**(1), 1–11.

Brandenburg, J.P. & van Keken, P.E., 2007. Deep storage of oceanic crust in a vigorously convecting mantle, *J. Geophys. Res. Solid Earth,* **112**(B6), B06403, doi:10.1029/2006JB004813.

Chernov, L.A., 1960. *Wave Propagation in a Random Medium,* Vol. 960, McGraw-Hill.

Cleary, J. & Haddon, R., 1972. Seismic wave scattering near the core-mantle boundary: a new interpretation of precursors to PKP, *Nature,* **240**(5383), 549–551.

Cormier, V.F., 1999. Anisotropy of heterogeneity scale lengths in the lower mantle from PKIKP precursors, *Geophys. J. Int.,* **136**(2), 373–384.

Cormier, V.F., 2000. D″ as a transition in the heterogeneity spectrum of the lowermost mantle, *J. geophys. Res. Solid Earth,* **105**(B7), 16 193–16 205.

Cormier, V.F. & Li, X., 2002. Frequency-dependent seismic attenuation in the inner core 2. A scattering and fabric interpretation, *J. geophys. Res. Solid Earth,* **107**(B12), ESE 14–1–ESE 14–15.

Doornbos, D., 1978. On seismic-wave scattering by a rough core-mantle boundary, *Geophys. J. R. astr. Soc.,* **53**(3), 643–662.

Doornbos, D. & Vlaar, N., 1973. Regions of seismic wave scattering in the Earth's mantle and precursors to PKP, *Nature,* **243,** 58–61.

Dziewonski, A.M. & Anderson, D.L., 1981. Preliminary Reference Earth Model, *Phys. Earth planet. Inter.,* **25**(4), 297–356.

Earle, P.S. & Shearer, P.M., 2001. Distribution of fine-scale mantle heterogeneity from observations of Pdiff coda, *Bull. seism. Soc. Am.,* **91**(6), 1875–1881.

Frost, D.A., Rost, S., Selby, N.D. & Stuart, G.W., 2013. Detection of a tall ridge at the core–mantle boundary from scattered PKP energy, *Geophys. J. Int,* doi:10.1093/gji/ggt242.

Haddon, R. & Cleary, J., 1974. Evidence for scattering of seismic PKP waves near the mantle-core boundary, *Phys. Earth planet. Inter.,* **8**(3), 211–234.

Hedlin, M.A. & Shearer, P.M., 2000. An analysis of large-scale variations in small-scale mantle heterogeneity using Global Seismographic Network recordings of precursors to PKP, *J. geophys. Res.,* **105**(B6), 13 655–13 673.

Hedlin, M.A. & Shearer, P.M., 2002. Probing mid-mantle heterogeneity using PKP coda waves, *Phys. Earth planet. Inter.,* **130**(3), 195–208.

Hedlin, M.A., Shearer, P.M. & Earle, P.S., 1997. Seismic evidence for small-scale heterogeneity throughout the Earth's mantle, *Nature,* **387**(6629), 145–150.

Kaneshima, S. & Helffrich, G., 2010. Small scale heterogeneity in the mid-lower mantle beneath the circum-Pacific area, *Phys. Earth planet. Inter.,* **183**(1–2), 91–103, Special Issue on Deep Slab and Mantle Dynamics.

Kennett, B.L.N. & Engdahl, E.R., 1991. Traveltimes for global earthquake location and phase identification, *Geophys. J. Int.,* **105**(2), 429–465.

Li, M. & McNamara, A.K., 2013. The difficulty for subducted oceanic crust to accumulate at the Earth's core-mantle boundary, *J. geophys. Res. Solid Earth,* **118,** 1807–1816.

Manga, M., 1996. Mixing of heterogeneities in the mantle: Effect of viscosity differences, *Geophys. Res. Lett.,* **23**(4), 403–406.

Margerin, L. & Nolet, G., 2003a. Multiple scattering of high-frequency seismic waves in the deep Earth: modeling and numerical examples, *J. geophys. Res. Solid Earth,* **108**(B5), 2234, doi:10.1029/2002JB001974.

Margerin, L. & Nolet, G., 2003b. Multiple scattering of high-frequency seismic waves in the deep Earth: PKP precursor analysis and inversion for mantle granularity, *J. geophys. Res.,* **108**(B11), 2514, doi:10.1029/2003JB002455.

Monnereau, M., Calvet, M., Margerin, L. & Souriau, A., 2010. Lopsided growth of Earth's inner core, *Science,* **328**(5981), 1014–1017.

Owens, T.J., Crotwell, H.P., Groves, C. & Oliver-Paul, P., 2004. SOD: Standing Order for Data, *Seismol. Res. Lett.,* **75**(4), 515–520.

Peng, Z., Koper, K.D., Vidale, J.E., Leyton, F. & Shearer, P., 2008. Inner-core fine-scale structure from scattered waves recorded by LASA, *J. geophys. Res* **113,** B09312, doi:10.1029/2007JB005412.

Rost, S. & Thomas, C., 2010. High resolution CMB imaging from migration of short-period core reflected phases, *Phys. Earth planet. Inter.,* **183**(12), 143–150, Special Issue on Deep Slab and Mantle Dynamics.

Sato, H. & Fehler, M.C., 1997. *Seismic Wave Propagation and Scattering in the Heterogeneous Earth,* Springer.

Shearer, P.M., 2007. Deep earth structure—seismic scattering in the deep Earth, in *Treatise on Geophysics,* pp. 695–729, ed. Schubert, G., Elsevier.

Shearer, P.M. & Earle, P.S., 2004. The global short-period wavefield modelled with a Monte Carlo seismic phonon method, *Geophys. J. Int.,* **158**(3), 1103–1117.

Shearer, P.M. & Earle, P.S., 2008. Observing and modeling elastic scattering in the deep Earth, *Adv. Geophys.,* **50,** 167–193.

Stixrude, L. & Lithgow-Bertelloni, C., 2012. Geophysics of chemical heterogeneity in the mantle, *Annu. Rev. Earth planet. Sci.,* **40**(1), 569–595.

Sun, D., Helmberger, D.V., Jackson, J.M., Clayton, R.W. & Bower, D.J., 2013. Rolling hills on the core–mantle boundary, *Earth planet. Sci. Lett.,* **361,** 333–342.

Vidale, J.E. & Hedlin, M.A., 1998. Evidence for partial melt at the core–mantle boundary north of Tonga from the strong scattering of seismic waves, *Nature,* **391**(6668), 682–685.